New Materials, Compounds and Applications
Vol.5, No.2, 2021, pp.79-86

MODELING THE PHASE DIAGRAM OF THE Tl_9GdTe_6 -Tl_4PbTe_3 -Tl_9BiTe_6 SYSTEM

S.Z. Imamaliyeva[1*], A.N. Mamedov[1,2], M.B. Babanly[1]

[1]Nagiyev Institute of Catalysis and Inorganic Chemistry of ANAS, Baku, Azerbaijan
[2]Azerbaijan Technical University, Baku, Azerbaijan

Abstract. The analytical multi-3D model of the phase diagram of the Tl_9GdTe_6-$Tl_8Pb_2Te_6$-Tl_9BiTe_6 system was obtained and visualized for the quasi-ternary and non-quasi-ternary high-temperature part. The analytical models of phase diagrams of the Tl_9GdTe_6 –$Tl_8Pb_2Te_6$ and Tl_9GdTe_6 –Tl_9BiTe_6 systems were obtained in the "temperature – composition" coordinates. The boundaries of the liquidus and solidus surface of crystallization of solid solutions and the $TlGdTe_2$ compound were obtained. The thermodynamic functions of mixing solid solutions were determined based on the model of regular solutions of non-molecular compounds. It was shown that solid solutions based on the ternary Tl_9GdTe_6, $Tl_8Pb_2Te_6$, and Tl_9BiTe_6 compounds have thermodynamic stability in the entire concentration range and the temperature range T = 300–780 K.

Keywords: *Phase diagram, thallium-gadolinium tellurides, thallium-lead tellurides, thallium-bismuth tellurides, 3D modeling.*

Corresponding Author: *Samira Imamaliyeva, Institute of Catalysis and Inorganic Chemistry named after acad. M.Nagiyev, ANAS, 113, H.Javid. ave., AZ-1143, Baku, Azerbaijan,*
e-mail: samira9597a@gmail.com

Received: *08 April 2021;* ***Accepted:*** *17 June 2021;* ***Published:*** *07 August 2021.*

1. Introduction

Chalcogenide rare-earth elements (REE) were studied for a long time due to their interesting physical properties such as superconductivity (Jha, 2014; Yarembash, 1975; Yumigeta *et al.*, 2021), mixed valences (Antonov, 2005), strong electron correlations (Kogar, 2020; Liu *et al.*, 2018), thermoelectric (Cheikh *et al.*, 2018; Wang *et al.*, 2011), magneto-optical properties (Yumigeta *et al.*, 2021; Boncher *et al.*, 2015; Guo, 2014; Verma, 2009; Xing *et al.*, 2020) et al. In particular, authors (Yumigeta *et al.*, 2021; Xing *et al.*, 2020) showed the promise for use of REE tritellurides in the high energy storage density, magnetic sensors, magnetic twistronic devices, and spintronics.

Development of methods for directed synthesis of new materials based on REE chalcogenides is based on reliable data on phase equilibria and thermodynamic data of the corresponding systems (Babanly *et al.*, 2017, 2019; Imamaliyeva, 2018a).

Subtelluride Tl_5Te_3which exhibits thermoelectric properties [Matsumoto et al., 2009] due to the peculiarities of the crystal lattice, has many ternary analogs of the types Tl_9AX_6 and Tl_4BX_3 (A-Sb, Bi, In, Au, REE; B-Sn, Pb, Mo, Cu, rare-earth elements; X-Se, Te) (Imamaliyeva, 2018a, 2020a, b; Wacker, 1991; Doert, 1994; Bradmöller, 1993, 1994a,b; Piasecki *et al.*, 2017; Plucinski *et al.*, 2015), also possessing several functional properties, namely optical (Piasecki *et al.*, 2017; Plucinski *et al.*, 2015), thermoelectric (Khan *et al.*, 2020; Guo, 2015), magnetic (Bangarigadu-Sanasy *et al.*, 2014; Isayeva *et* al., 2020), as well as topological insulators properties (Arpino *et al.*, 2015; Niu *et al.*,

2014). In recent years, to improve thermoelectric performance, intensive work has been carried out to study solid solutions and doped phases based on these compounds (Khan *et al.*, 2020; Guo *et al.*, 2014a).

To obtain new variable composition phases with Tl_5Te_3-structure, we studied phase relations in some systems consisting of Tl_5Te_3 and its ternary analogs (Imamaliyeva *et al.*, 2018b; Babanly *et al.*, 2008; Imamaliyeva *et al.*, 2017a, b). It was obtained that studied systems are characterized by the formation of continuous series of solid solutions at the solidus temperatures and below, which are crystallized in the tetragonal Tl_5Te_3 structure type.

As a continuation of the studies of the listed systems, in (Imamaliyeva *et al.*, 2020c; Imamaliyeva *et al.*, 2021) the 3D modeling of the phase diagrams of the Tl_9SmTe_6-Tl_4PbTe_3-Tl_9BiTe_6 and Tl_9TbTe_6-Tl_4PbTe_3-Tl_9BiTe_6 systems was carried out.

The purpose of this article is 3D modeling of the phase diagram of the Tl_9GdTe_6 – Tl_4PbTe_3–Tl_9BiTe_6 system based on the phase diagrams of the Tl_9GdTe_6 –Tl_4PbTe_3 and Tl_9GdTe_6 –Tl_9BiTe_6 systems using the DTA data of the ternary system.

2. Experiments and results

2.1. Boundary systems

To modeling the Tl_9GdTe_6-$2Tl_4PbTe_3$-Tl_9BiTe_6 ternary system, the analytical approximation of the liquidus and solidus of the boundary Tl_9GdTe_6 -$2Tl_4PbTe_3$ and Tl_9GdTe_6-Tl_9BiTe_6 systems is necessary. The analytical approximation of the liquidus and solidus of the third boundary $2Tl_4PbTe_3$-Tl_9BiTe_6 system was carried out in (Imamaliyeva *et al.*, 2020c). To equalize the number of atoms in the formulas of initial compounds, the thallium–lead-tellurium compound was taken as a dimer $2Tl_4PbTe_3$. To modeling of the Tl_9GdTe_6-$2Tl_4PbTe_3$ and Tl_9GdTe_6 -Tl_9BiTe_6 systems, we used the experimental results of Babanly et al, (2008). According Babanly et al. (2008), these cross-sections are characterized by the formation of continuous solid solutions (δ-phase) with the Tl_5Te_3 structure. The Tl_9GdTe_6-$2Tl_4PbTe_3$ and Tl_9GdTe_6 -Tl_9BiTe_6 systems are non-quasi-binary due to the incongruent melting character of the Tl_9GdTe_6 compound. As a result, in a wide compositions interval (up to 60 mol% Tl_9GdTe_6), the $TlGdTe_2$ compound first crystallizes from the melt, which leads to the formation of L+$TlGdTe_2$ two-and L + $TlGdTe_2$ + δ three-phase areas. Below the solidus, all boundary systems are quasi-binary.

For the analytical description of the liquidus and solidus of the Tl_9GdTe_6 -$2Tl_4PbTe_3$ and Tl_9GdTe_6-Tl_9BiTe_6 systems, the technique described in Imamalıyeva et al. (2020c; 2021) was used. The temperature dependence of the liquidus and solidus on the composition for these systems has the following forms (equations are represented in computer form).

For alloys (1-*x*)($Tl_8Pb_2Te_6$)– *x*(Tl_9GdTe_6):

$$T\ (liq)= 893.98-53.3*x-40.48*x\text{^}2 \quad (1)$$

$$T\ (sol)= 892.6-138.2*x-45.77*x\text{^}2 \quad (2)$$

$$T\ (liq, TlGdTe_2)= -840+3989*x-1961*x\text{^}2 \quad (3)$$

For alloys (1-*x*)(Tl_9BiTe_6)– *x*(Tl_9GdTe_6):

$$T(liq)= 830-30*x+4.113*x+11.31*x\text{^}2-15.328*x\text{^}3 \quad (4)$$

$$T(sol)= 830-30*x-8.16*x+7.568*x\text{^}2+0.54*x\text{^}3 \quad (5)$$

$$T(liq, TlGdTe_2)=963.5-3210*x+7185.7*x\text{^}2-3750*x\text{^}3 \quad (6)$$

Equations (1-6) are visualized in Fig. 1:

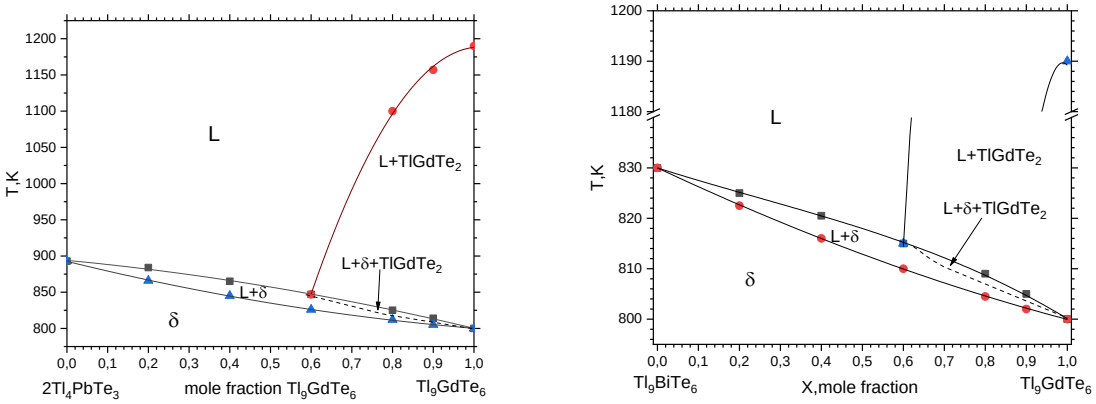

Figure 1. Phase diagram of the Tl_9GdTe_6 -$2Tl_4PbTe_3$ and Tl_9GdTe_6-Tl_9BiTe_6 systems: symbols are results of Babanly et al. (2018), curves are visualized by equations (4-6)

2.2. Ternary system

For the 3D modeling of the liquidus and solidus surfaces of the Tl_9GdTe_6 - $2Tl_4PbTe_3$ -Tl_9BiTe_6 ternary system, the following equations are used:

$$T(liq.)=yT_{liq}(1-2)+(1-y)T_{liq}(1-3)+ay(1-y)(1-x)^2 \quad (7)$$

$$T(liq, TlGdTe_2)=yT_{liq}(1-2)+(1-y)T_{liq}(1-3)+by(1-y)(1-x)^2 \quad (8)$$

$$T(solidus)=yT_{sol}(1-2)+(1-y)T_{sol}(1-3)+T_{sol}(2-3)+cy(1-y)(1-x)^2 \quad (9)$$

Here, the compounds are designated: 1-Tl_9CdTe_6; 2- ($2Tl_4PbTe_3$); 3-Tl_9BiTe_6. x-is the mole fraction of the component 1, $y = x_2 / (1-x)$; $(1-y) = x_3 / (1-x)$; x_2, x_3-mole fraction of compounds 2 and 3. Parameters a, b, c are determined based on differential thermal analysis (DTA) data for the studied ternary system.

Inserting relations (1-6) into (7-9) we get:

$$T(liq.) = (893.98-53.3*x-40.48*x\text{^}2)*y+(830-30*x+4.113*x+ +11.31*x\text{^}2-15.328*x\text{^}3)*(1-y)+40*y*(1-y)*(1-x) \quad (10)$$

$$T(sol.)=(892.6-138.2*x+45.77*x\text{^}2)*y+(830-30*x-8.16*x+ +7.568*x\text{^}2+0.54*x\text{^}3)*(1-y)+44*y*(1-y)*(1-x)\text{^}2 \quad (11)$$

$$T(liq.,TlGdTe_2)=(-840+3989*x-1961*x\text{^}2)*y+(963.5-3210*x+ 7185.7*x\text{^}2-3750*x\text{^}3)*(1-y) \quad (12)$$

In equations (10-12) and in Fig.2: x – is mol. fractions of Tl_9GdTe_6; x_2 and x_3 are mol. fractions of Tl_8PbTe_3 and Tl_9BiTe_6; $y = x_2 / (1-x)$. In equations (11,12): $x = 0 \div 1$; $y = 0 \div 1$. In equation (12): $x = 0.65 \div 1$; $y = 0 \div 1$. Equations (10-12) are visualized in Fig. 2,3:

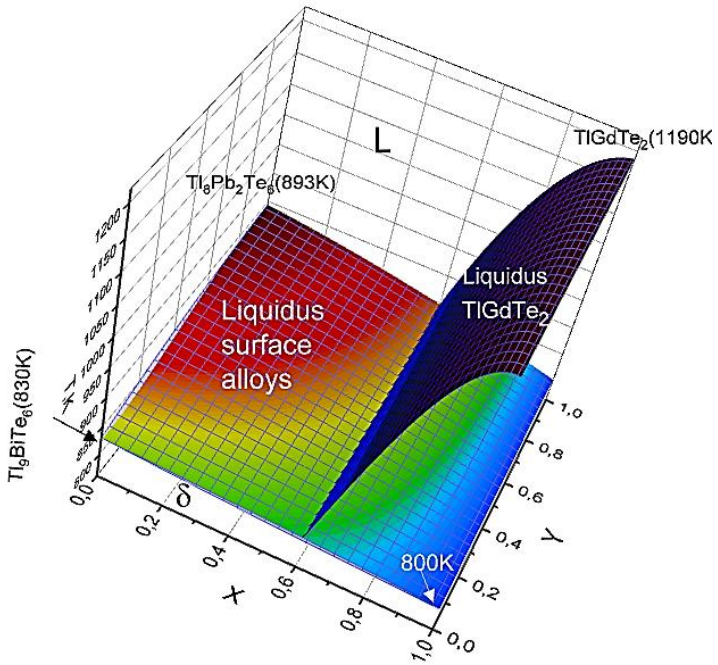

Figure 2. 3D model of the phase diagram of theTl_9GdTe_6 -$2Tl_4PbTe_3$ -Tl_9BiTe_6 system vizualized by equations (10-12)

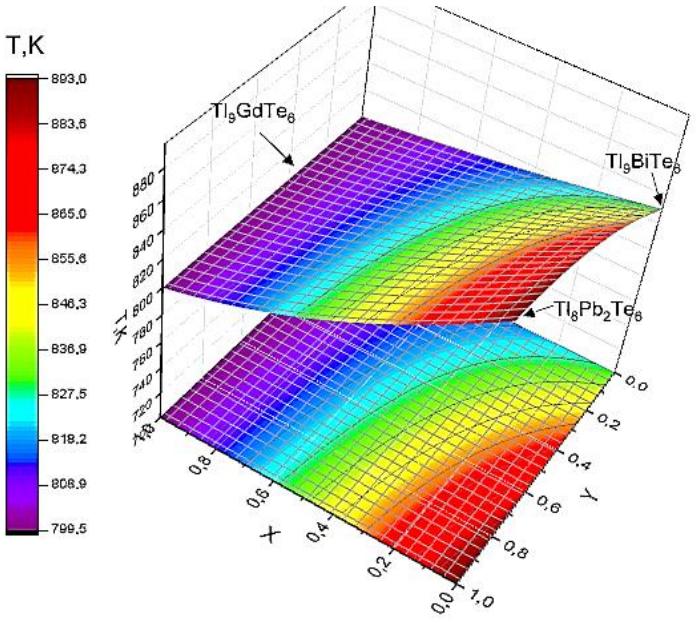

Figure 3. 3D model and projection of the solidus surface of solid solutions in the Tl_9GdTe_6 - $2Tl_4PbTe_3$ -Tl_9BiTe_6 system visualized by equation (11)

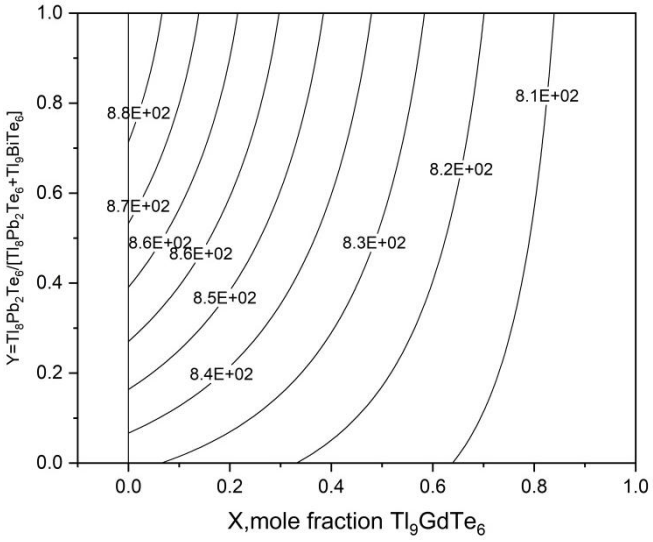

Figure 4. Temperature contours for solid solutions in the Tl_9GdTe_6 -$2Tl_4PbTe_3$ -Tl_9BiTe_6 system. Designation E + 02 means 10^2

2.3. Stability of solid solutions

To calculate the free energy of formation of solid solutions of the boundary systems, an asymmetric version of the model of regular solutions was used, which has been successfully tested in (Mamedov, 2015; Imamaliyeva *et al.*, 2021):

$$\Delta G_T^0 = (a + bT)x^m(1-x)^n + RT[pxlnx + q(1-x)\ln(1-x)] \qquad (13)$$

Here the first term represents the enthalpy of mixing of solid solutions in an asymmetric version of the model of regular solutions. For solid solutions with unlimited solubility, the mixing parameter is $a< 0$; $b> 0$ the second term is the configurational entropy of mixing solid solutions according to the model of non-molecular compounds (Mamedov, 2015); p and q are a number of different atoms in compounds, R= 8.314 $Jmol^{-1}$ K^{-1}.

In equation (13) it is necessary to determine the parameter of the intermolecular interaction a and the degree of concentration m, n. For the model of strictly regular solutions, $m = n = 1$. To approximate the thermodynamic function of formation, an asymmetric version of the model of regular solutions ($m \neq n \neq 1$) should be used. To solve the equation containing two functional parameters (temperature, composition) and Gibbs excess free energy, the Multipurpose Genetic Algorithm was used (Preuss *et al.*, 2015). The following conditions were used to carry out the iteration process:

$$x=0\div1;\ a<0\ ;b>0;\ m>n>1\ ;\ 300K<T<780K$$

To determine the thermodynamic stability of solid solutions, the Lupis internal stability function (Mamedov *et al.*, 1996) was used:

$$\Psi = x(1-x)\frac{d^2(\Delta G/RT)}{dx^2} \qquad (14)$$

It was found that $\Psi> 0$ in the 300-780 K temperature range in the entire range of concentrations. Hence it shows the thermodynamic stability of solid solutions in the entire interval of concentrations within 300-780 K temperature interval.

3. Conclusion

The analytical multi-3D model of the phase diagram of the Tl_9GdTe_6-$Tl_8Pb_2Te_6$-Tl_9BiTe_6 system was obtained and visualized for the quasi-ternary and nonquasi-ternary high-temperature part. For the Tl_9GdTe_6 –$Tl_8Pb_2Te_6$ and Tl_9GdTe_6 –Tl_9BiTe_6 boundary systems, the analytical models of phase diagrams of the systems were obtained in forms of temperature dependence on the composition, and their graphs are built. The thermodynamic functions of solid solutions mixing were determined using the model of regular solutions of non-molecular compounds. It was found that in the entire concentration range in the temperature range T = 300–780 K, the second derivative of the integral mixing free energy is greater than zero. Therefore, the values of the stability function are also greater than zero ($\Psi > 0$) in the entire range of concentrations, which indicates the thermodynamic stability of solid solutions.

Acknowledgments

The work has been carried out within the framework of the international joint research laboratory "Advanced Materials for Spintronics and Quantum Computing" (AMSQC) established between the Institute of Catalysis and Inorganic Chemistry of ANAS (Azerbaijan) and Donostia International Physics Center (Basque Country, Spain) and partially supported by the Science Development Foundation under the President of the Republic of Azerbaijan, a grant EİF/MQM/Elm-Tehsil-1-2016-1(26)-71/01/4-M-33.

References

Antonov, V.N., Harmon, B.N., & Yaresko, A.N. (2005). Electronic structure of mixed-valence and charge-ordered Sm and Eu pnictides and chalcogenides. *Phys. Rev. B.*, *72*(8), 085119.

Arpino, K.E., Wasser, B.D., & McQueen, T.M. (2015). Superconducting Dome and Crossover to an Insulating State in $[Tl_4]Tl_{1-x}Sn_xTe_3$. *APL Mater*, *3*(4), 041507-041508.

Babanly, M.B., Chulkov, E.V., Aliev, Z. S., Shevelkov, A.V., & Amiraslanov, I.R. (2017). Phase diagrams in materials science of topological insulators based on metal chalcogenides. *Russ. J. Inorg. Chem.*, *62*(13), 1703–1729.

Babanly, M.B., Mashadiyeva, L.F., Babanly, D.M., Imamaliyeva, S.Z., Taghiyev, D.B., & Yusibov, Y.A. (2019). Some aspects of the complex investigation of the phase equilibria and thermodynamic properties of the ternary chalcogenide systems by the EMF method. *Russ. J. Inorg. Chem.*, *64*(13), 1649-1671.

Babanly, M.B., Dashdiyeva, G.B., & Huseynov, F.N. (2008). Phase equilibriums in the Tl_4PbTe_3-Tl_9BiTe_6 system. *Chem.Probl.*, *1*, 69-72.

Bangarigadu-Sanasy, S., Sankar, C.R., Dube, P.A., Greedan, J.E., & Kleinke, H. (2014). Magnetic properties of Tl_9LnTe_6, Ln = Ce, Pr, Tb, and Sm. *J. Alloys Compd.*, *589*, 389–392.

Boncher, W., Dalafu, H., Rosa, N., & Stoll, S. (2015). Europium chalcogenide magnetic semiconductor nanostructures. *Coord. Chem. Rev*., *289–290*(1), 279-288.

Bradtmöller, S., & Böttcher, P. (1993). Darstellung und kristallostructur von $SnTl_4Te_3$ und $PbTl_4Te_3$. *Z. Anorg. Allg. Chem.*, *619*, 1155-1160.

Bradtmöller, S., & Böttcher, P. (1994a). Crystal structure of copper tetra thallium tritelluride $CuTl_4Te_3$. *Z. Kristallogr*., *209*(1), 97.

Bradtmöller, S., & Böttcher, P. (1994b). Crystal structure of molybdenum tetra thallium tritelluride, $MoTl_4Te_3$. *Z. Kristallogr*., *209*(1), 75.

Cheikh, D., Hogan, B.E., Vo, T., Allmen, P., Lee, K., Smiadak, D.M., Zevalkink, A., Dunn, B.S., Fleurial, J.P., & Bux, S.K. (2018). Praseodymium Telluride: A High Temperature. High ZT Thermoelectric Material. *Joule*, *2*, 698–709.

Doert, T., & Böttcher, P. (1994). Crystal structure of bismuth nonathalliumhexatelluride $BiTl_9Te_6$. *Z.Kristallogr.*, *209*, 95.

Guo, S-P., & Guo, G-C. (2014a). Crystal structure and magnetic and photocatalytic properties of a new ternary rare-earth mixed chalcogenide, $Dy_4S_4Te_3$. *J. Mater. Chem. A*, 2, 20621-20628.

Guo, Q., & Kleinke, H. (2015). Thermoelectric properties of hot-pressed (Ln=La, Ce, Pr, Nd, Sm, Gd, Tb) and $Tl_{10-x}La_xTe_6$ ($0,90<x<1,05$). *J. Alloys Compd.*, *630*, 37-42.

Guo, Q., Assoud, A., & Kleinke, H. (2014). Improved Bulk Materials with Thermoelectric Figure-of-Merit Greater than 1: $Tl_{10}–xSn_xTe_6$ and $Tl_{10}–xPb_xTe_6$. *Adv. Energy Mater.*, *4*(14), 1400348-8.

Imamaliyeva, S.Z. (2018a). Phase diagrams in the development of thallium-REE tellurides with Tl_5Te_3 structure and multicomponent phases based on them**.** *Condensed Matter and Interphases*, *20*(3), 332–347.

Imamaliyeva, S.Z. (2020a). New thallium tellurides with rare earth elements. *Condensed Matter and Interphases*. *4*, 460-465.

Imamaliyeva, S.Z. (2020b). Tl_4GdTe_3 and Tl_4DyTe_3 - Novel Structural Tl_5Te_3 Analogues. *Phys. Chem. Solid State*, *21*(3), 492-495.

Imamaliyeva, S. Z. Alakbarzade, G.I., Mamedov, A.N., Taghiyev, D.B., & Babanly, M.B. (2020c). Modeling the Phase Diagram of the Tl_9SmTe_6-Tl_4PbTe_3-Tl_9BiTe_6 System. In book: *14th International Conference on Theory and Application of Fuzzy Systems and Soft Computing* – ICAFS, 480-489.

Imamaliyeva, S.Z., Alakbarzade, G.I., Mamedov, A.N., & Babanly, M.B. (2021). Modeling the phase diagram of the Tl_9TbTe_6 -Tl_4PbTe_3 -Tl_9BiTe_6 system. *Azerb. Chem. J.*, 3, 6-12.

Imamaliyeva, S.Z., Alakbarzade, G.I., Salimov, Z.E., Izzatli, S.B., Jafarov, Ya.I., & Babanly, M.B. (2018b). The Tl_4PbTe_3-Tl_9GdTe_6-Tl_9BiTe_6 isopleth section of the Tl-Pb-Bi-Gd-Te system. *Chem.Probl.*, *4*, 495-504.

Imamaliyeva, S.Z., Gasanly, T.M., Amiraslanov,I.R., & Babanly, M.B. (2017a). Phase relations in the Tl_5Te_3-Tl_9SbTe_6-Tl_9TbTe_6 system. *Chem. Chem.Technol*, *11*(4), 415-419.

Imamaliyeva, S.Z., Gasanly, T.M., Zlomanov, V.P., & Babanly, M.B. (2017b). Phase equilibria in the Tl_5Te_3–Tl_9BiTe_6–Tl_9TbTe_6 system. *Inorg. Mater.*, *53*(7), 685-689.

Isaeva, A., Schönemann, R., & Doert, T. (2020). Syntheses, crystal structure and magnetic properties of Tl_9RETe_6 (RE=Ce, Sm, Gd*). Crystals*, *10*(4), 1-11.

Jha, A.R. (2014). *Rare Earth Materials: Properties and Applications*. United States; CRC Press.

Khan, W.M., Rahman, A.U., Tufail, M., Ibrar, M., Shah, W.H., Syed, W.A., & Gul, B. (2020). Toward controlled thermoelectric properties of Pb and Sb co-doped nanostructured Thallium Telluride for energy applications. *Mater. Res. Express.*,*7*, 105010-105013.

Kogar, A. (2020). Light-induced charge density wave in $LaTe_3$. *Nature Physics*, *16*(2), 1-5.

Liu, W., Zhang, Z., Ji, J., Liu, Y., Li, J., Wang, X., Lei, X., Chen, G., & Zhang, Q.(2018). Rare-Earth Chalcogenides: A Large Family of Triangular Lattice Spin Liquid Candidates. *Chinese Phys. Lett.*, *35*(11), 117501.

Mamedov, A.N. (2015). *Thermodynamics of Systems with Non-Molecular Compounds*. LAP Germany, 124 p.

Mamedov, A.N., Mekhdiev, I.H., Agaeva, S.A., & Gulieva, S.A. (1996). Calculation of the adsorption of binary alloy components using the stability function. *Russ. J. Phys. Chem. A.*, *70*(8), 1455-1457.

Matsumoto, H., Kurosaki, K., Muta, H., & Yamanaka, Sh. (2009). Thermoelectric Properties of the Thallium-Tellurium Binary Compounds. *Mater. Transact.*, *50*(7), 1582-1585.

Niu, C., Dai, Y., Huang, B., Bihlmayer, G., Mokrousov, Y., Wortmann, D., & Blügel, S. (2014). Natural three-dimensional topological insulators in Tl_4PbTe_3 and Tl_4SnTe_3. *Frühjahrstagung der Deutschen Physikalischen Gesellschaft*, 01899.

Piasecki, M., Brik, M.G., & Barchiy, I.E. (2017). Band structure, electronic and optical features of Tl_4SnX_3 (X= S, Te) ternary compounds for optoelectronic applications. *J. Alloys Compd., 710,* 600-607.

Plucinski, K.J., Sabov, M.Y., Fedorchuk, A.O., Barchiy, I., & Lakshminarayana, G. (2015). UV laser induced second order optical effects in the Tl_4PbTe_3, Tl_4SnSe_3 and Tl_4PbSe_3 single crystals. *Opt. Quant. Electron.,47*(2), 185-192.

Preuss, M., Wessing, S., Rudolph, G., & Sadowski, G. (2015). Solving phase equilibrium problems by means of avoidance-based multiobjectivization. In *Springer handbook of computational intelligence*. Part E.58, Evol. Comput. P. 1159-1169.

Verma, A.S. (2009). Electronic and Optical Properties of Rare-earth Chalcogenides and Pnictides. *African Phys.Rev., 3*, 11-20.

Wacker, K. (1991). Die kristalstrukturen von Tl_9SbSe_6 und Tl_9SbTe_6. *Z. Kristallogr. Supple, 3*, 281.

Wang, X., Yang,R., Zhang, Y., Zhang, P., & Xue, Y. (2011). Rare earth chalcogenide Ce_3Te_4 as high efficiency high temperature thermoelectric material. *Appl. Phys. Lett., 98*, 222110.

Xing, Y., Li,Y., Yang, Z., Wang,Z., Yang,P., Ge,J., Liu,Y., Liu,Y., Luo,T., Tang,Y., & Wang, J.(2020). Extremely large and anisotropic magnetoresistance in rare-earth tritelluride $TbTe_3$. *J. Appl. Phys., 128*, 073901.

Yarembash, E.I., & Eliseev, A.A. (1975). *Chalcogenides of Rare-Earth Elements* Nauka, Moscow (in Russian).

Yumigeta, K., Qin, Y., Li, H., Blei, M., Attarde, Y., Kopas, C., &Tongay, S. (2021). Advances in Rare-Earth Tritelluride Quantum Materials: Structure, Properties, and Synthesis. *Adv. Sci.*, 2004762-17.